ECS The Electrochemical Society
Advancing solid state & electrochemical science & technology

OPEN ACCESS

Battery Degradation-Aware Current Derating: An Effective Method to Prolong Lifetime and Ease Thermal Management

CrossMark

Battery Degradation-Aware Current Derating: An Effective Method to Prolong Lifetime and Ease Thermal Management

Michael Schimpe,[1,=,*,z] Jorge V. Barreras,[2,3,=] Billy Wu,[2,4] and Gregory J. Offer[2,3,*]

[1]Visiting Researcher, Imperial College London, United Kingdom
[2]The Faraday Institution, Didcot, United Kingdom
[3]Department of Mechanical Engineering, Imperial College London, United Kingdom
[4]Dyson School of Design Engineering, Imperial College London, United Kingdom

To ensure the safe and stable operation of lithium-ion batteries in battery energy storage systems (BESS), the power/current is derated to prevent the battery from going outside the safe operating range. Most derating strategies use static limits for battery current, voltage, temperature and state-of-charge, and do not account for the complexity of battery degradation. Progress has been made with models of lithium plating for fast charging. However, this is a partial solution, does not consider other degradation mechanisms, and still requires complex optimization work, limiting widespread adoption. In this work, the calendar and cycle degradation model is analysed offline to predetermine the degradation rates. The results are integrated into the current-derating strategy. This framework can be adapted to any degradation model and allows flexible tuning. The framework is evaluated in simulations of an outdoors-installed BESS with passive thermal management, which operates in a residential photovoltaic application. In comparison to standard derating, the degradation-aware derating achieves: (1) increase of battery lifetime by 65%; (2) increase in energy throughput over lifetime by 49%, while III) energy throughput per year is reduced by only 9.5%. These results suggest that the derating framework can become a new standard in current derating.

Battery energy storage systems (BESS) are a technical option for the renewable energy transition, with lithium-ion (Li-ion) batteries currently being a highly important battery technology. The economics of a Li-ion BESS are strongly correlated with battery lifetime, which is typically measured by the number of cycles or years of operation achievable.[1]

The high cost of batteries and their limited lifetime, explains why many active methods to increase battery lifetime can be found in the literature. They aim to control, in some way, temperature, voltage, state-of-charge (SOC) or current, all of which are main drivers for battery degradation.[2–5] These approaches may involve derating strategies,[6,7] thermal management,[8–14] hybridization,[15–20] active balancing and by-passing/reconfiguration.[21–26] Numerous studies focus on the optimization of lithium plating and fast-charging, which can be considered as a specific form of current derating.[27–30]

Derating is the operation of an electrical or electronic device at less than its rated maximum capability to ensure safety, extend lifetime or avoid system shutdown.[6,31] Figure 1 shows an example of a simple temperature-based derating strategy for Li-ion batteries commonly used in industry.[6]

The manufacturer's data sheet provides hard limits for the operating area, in terms of currents, voltages, or temperatures, which define the battery Safe Operating Area (SOA). To prolong battery lifetime using simple standard derating strategies, more restrictive static limits than the SOA can be set, but this leads to reducing battery performance more frequently and intensively. A literature review (Section 1.1) discusses the available work on battery lifetime prognosis and maximization in detail.

In this work, we present a framework for integrating a battery degradation model into a current-derating control strategy. Hereby, the complex degradation mechanisms are accurately accounted for in the calculation of the maximum battery current, enabling precise derating during operation. Details on the novelty are outlined in section 1.2. After a general model-based evaluation of battery degradation (Section 2), the control strategy is developed (Section 3). To validate and illustrate the significance of degradation-aware derating the control strategy is investigated in a simulation of a residential photovoltaic-buffer BESS (Section 4).

Literature review.—As reported by Barreras et al.[6] and Sun et al.,[7] there is a lack of guidelines and frameworks for derating Li-ion batteries in the literature. On the other hand, many derating guidelines exist for other electronic components, such as lead-acid batteries,[32] microprocessors,[33] or integrated circuits.[34]

Sun et al. presented guidelines for Li-ion batteries using temperature, discharge currents, charge currents, charge cut-off current, charge cut-off voltage, and SOC stress factors to reduce the rate of capacity loss in operation.[7] But these guidelines require a transfer into a framework, i.e. a control strategy, for battery management systems (BMS) or system operators to improve battery operation/lifetime. In that sense, Barreras et al. presented simple derating frameworks that are the current industry standard for Li-ion batteries. These are typically algorithms that limit the current of the battery during charging or discharging to prevent operation outside certain operating area, bounded by static SOC, voltage, or temperature limits.[6]

While in some scenarios tuning these simple derating strategies can be effective, as recently shown by Sowe et al.[35] for islanded microgrids, they always present a major caveat: they are empirical, i.e. based on what is experienced or seen in the field or simulations rather than on solid theoretical foundation. This means that they are case-specific solutions, which should be re-evaluated each time.

With regard to active thermal management technologies, in theory, they enable control of the battery temperature closer to the optimal operational level in terms of battery lifetime. However, in practice, the standard strategy for active thermal management is basically to maintain a constant operating temperature around 15 °C–25 °C, and this does not ensure minimum degradation.[4,36] Also, active thermal management may consume substantial energy, resulting in e.g. 1%–2%-points reduction of energy efficiency,[37] and require maintenance, increasing investment and operational costs. Conversely, a BESS with passive or limited systems will have lower capital and operating costs, but it may also exhibit reduced lifetime and derated performance when is used in unfavourable conditions.[2–5] Thus, the value proposition for thermal management in BESS is challenging and engineers need to find compromise solutions.

=These authors contributed equally to this work.
*Electrochemical Society Member.
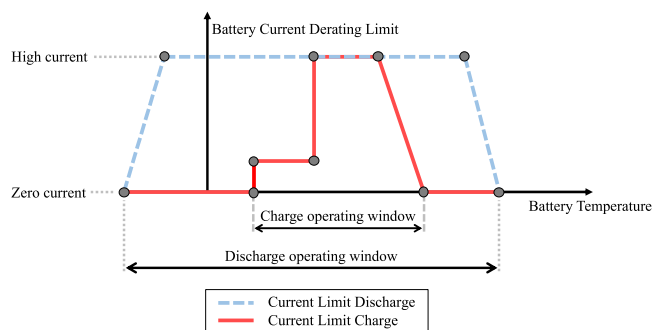zE-mail: michael.schimpe@gmail.com

Figure 1. Exemplary simple temperature-based derating strategy. Adapted from Ref. 6.

Similar reasoning can be done with respect to hybridization, advanced balancing systems, or by-passing/re-configuration, which can enhance the BESS performance and lifetime through current control but may increase costs. In principle, this makes all these active solutions less suitable for a low-cost BESS.

Among all these active approaches to prolong battery lifetime, derating is the only one that does not increase costs. Furthermore, all those active methods, except for derating, may influence system reliability and generate safety issues. For instance, active thermal management systems may have faulty fans,[38] leakage of cooling liquids,[39] or defects of electronic components.[40]

Nowadays, there is significant room for improvement in derating strategies, since the standard approaches are not only simple but simplistic, since they do not take into account the complexity of the battery degradation mechanisms.

To deal with the complexity of battery degradation, many models have been proposed in the literature. They predict battery lifetime based on estimations of the degradation rate, in terms of capacity fade or internal resistance increase, from a combination of operating conditions, e.g. time, SOC, current and/or temperature values. There are three main approaches: (1) physicochemical models,[41–44] which are based on first principles and require in-depth modelling and parametrization of degradation mechanisms, (2) purely empirical models, which require extensive experimental testing, and can be used to evaluate calendar degradation,[2,45,46] cycle degradation[47–49] or superimposed calendar and cycle degradation,[50–53] and (3) semi-empirical models, which are a combination of both.[1,3,4,54] Degradation models are often used offline to evaluate battery lifetime, for example, in residential BESSs, by Mishra et al.,[55] Smith et al.,[10] or Sowe et al.[35]

On the other hand, some papers have also evaluated the use of degradation models to improve system-level operating strategies, particularly during charging. In our view, these should be referred to as degradation-aware derating strategies, but there is no standardized nomenclature so far. For example, such derating strategies were evaluated in stationary BESS by Patsios et al.,[41] who focused on the SOC, and Angenendt et al.,[56] who focused on forecasting the battery operation. Also, optimized control of grid-connected BESS through the combination of optimization methods with battery and degradation models was evaluated by Reniers et al.,[57] and Goebel et al.,[58] who compared different BESS control optimization approaches with respect to battery degradation. An ageing aware energy management system was also proposed by Kumtepeli et al.[59]. Schimpe et al.[60] evaluated efficiency- and degradation-aware BESS control based on the marginal costs of system operation. Such an approach was further extended with a focus on operation optimization using Mixed Integer Linear Programming by Hesse et al.[61] and Kumtepeli et al.[62]. Finally, numerous charging current optimization studies exist which calculate the maximum fast-charging current while avoiding especially lithium plating.[27–30]

However, all these solutions may be seen as partial, focusing only on charging/specific effects, and complex. They require combining battery and degradation models with online/offline optimization methods, and require optimization algorithms and/or forecast algorithms. Thus their application in real-time systems is possibly limited.

Contribution of this work.—In contrast, for the first time in the literature, here we use the calendar and cycle degradation model offline to predetermine the degradation rates through parameter sweeps, and then, we integrate these results online through simple look-up tables.

Regarding cycle ageing, the model is run offline iteratively to find the degradation rates for each combination of SOC, temperature and current. From those results, a first look-up table is generated, which retrieves the maximum allowable battery current regarding cycle ageing from the actual SOC, temperature, and cycle degradation rate limit, defined in terms of capacity loss per cycle.

Similarly, for calendar ageing, the model is run offline iteratively to find the degradation rates for each SOC and temperature. From these data, a second look-up table is created, which retrieves the maximum allowable battery temperature from the actual SOC, and calendar degradation rate limit, defined in terms of capacity loss per hour. From that temperature and using an electro-thermal battery model, the allowable battery current limit regarding calendar ageing is calculated.

All derating calculations, offline before operation and during operation, are performed with the actual SOC.

This is a flexible framework, which can be adapted to any degradation model, and allows easy-tuning of the online algorithm, which becomes more or less restrictive depending on the degradation rate limits for cycle and calendar degradation. The degradation rate limits can be defined individually by the user, the BMS, or the system-operator. Also, the algorithm only demands commonly monitored parameters during operation, namely battery and ambient temperature and SOC, and does not require a forecast of the system load in the future.

In this paper, we use a semi-empirical degradation model previously developed by Schimpe et al.[3,4,54] The model is validated over a wide range of operating conditions, is applicable due to its accuracy, takes main degradation mechanisms into account, and evaluates degradation separately for calendar and cycle ageing. It is worth noting that this model considers only capacity loss, and neglects effects on power capability or internal resistance. That is because the latter was found to be negligible for the chosen lithium iron phosphate/graphite cell after extensive testing, however, this may not be the case for other cells.

This novel framework was introduced by the authors for the first time in Ref. 63. In this paper, we offer a comprehensive description and evaluation through simulations. The target application considered is a residential PV buffer BESS. The BESS is charged using excess power from the PV system when the PV power production exceeds the household consumption, and it is discharged when the household consumption cannot be supplied from the PV system. The evaluated system features passive cooling and is installed outdoors, being exposed to ambient temperature variations. Consequently, unfavourable operating conditions for the battery cells are expected, which are particularly interesting to reveal the full potential of the proposed derating strategy. The system is evaluated in year-round simulations to analyse seasonal variations. Results are promising, showing a significant positive impact on battery lifetime, which is almost doubled, with a minor influence on battery performance.

Model-Based Capacity Loss Evaluation Under Constant Conditions

The implemented degradation model developed by Schimpe et al.[4] is parametrized for a 3 Ah lithium iron phosphate/graphite cylindrical cell manufactured by SONY. This chemistry and the specific cell is suitable for stationary BESS.[64]

The degradation model calculates the relative total capacity loss Q_{Loss} due to calendar ageing, $Q_{L,\text{Cal}}$, and cycle ageing, $Q_{L,\text{Cyc}}$.

Cycle ageing capacity loss is calculated as sum of the loss mechanisms due to cycling at high temperature linked to increased solid-electrolyte interphase (SEI) growth ($Q_{L,\text{Cyc,High }T}$), low temperature ($Q_{L,\text{Cyc,Low }T}$), and low temperature at high SOC ($Q_{L,\text{Cyc,Low }T \text{ High SOC}}$), linked to lithium plating:

$$Q_{\text{Loss}}(T_{\text{Cell}}, SOC, I_{\text{Ch}}, Q_{\text{Tot}}, Q_{\text{Ch}}, t) = Q_{L,\text{Cal}}(T_{\text{Cell}}, SOC, t)$$
$$+ Q_{L,\text{Cyc,High }T}(T_{\text{Cell}}, Q_{\text{Tot}})$$
$$+ Q_{L,\text{Cyc,Low }T}(T_{\text{Cell}}, I_{\text{Ch}}, Q_{\text{Ch}})$$
$$+ Q_{L,\text{Cyc,Low T High SOC}}(T_{\text{Cell}}, I_{\text{Ch}}, SOC, Q_{\text{Ch}}) \quad [1]$$

The calendar ageing capacity loss, $Q_{L,\text{Cal}}$, is calculated as a function of time and the calendar degradation stress factor, k_{Cal}, which in turn is a function of battery temperature T_{Cell} and battery SOC.

The cycle ageing capacity loss due to high-temperature effects, $Q_{L,\text{Cyc,High }T}$, is calculated as function of the total charge throughput of the battery during charging and discharging, Q_{Tot}, and the degradation stress factor $k_{\text{Cyc,High }T}$, which is a function of the battery temperature T_{Cell}.

The cycle ageing capacity loss due to low-temperature effects, $Q_{L,\text{Cyc,Low }T}$, is driven through charge operation only. It is calculated as a function of the charge throughput of the battery during charging operation, Q_{Ch}, and the degradation stress factor, $k_{\text{Cyc,Low }T}$, which is a function of battery temperature T_{Cell} and battery charge current I_{Ch}.

Finally, the cycle ageing capacity loss at low temperature and high SOC, $Q_{L,\text{Cyc,Low }T \text{ High SOC}}$, is calculated similarly, but featuring an additional dependency on SOC in the degradation stress factor, $k_{\text{Cyc,Low }T \text{ High SOC}}$.

$$Q_{\text{Loss}}(T_{\text{Cell}}, SOC, I_{\text{Ch}}, Q_{\text{Tot}}, Q_{\text{Ch}}, t) = k_{\text{Cal}}(T_{\text{Cell}}, SOC) \cdot \sqrt{t}$$
$$+ k_{\text{Cyc,High T}}(T_{\text{Cell}}) \cdot \sqrt{Q_{\text{Tot}}}$$
$$+ k_{\text{Cyc,Low }T}(T_{\text{Cell}}, I_{\text{Ch}}) \cdot \sqrt{Q_{\text{Ch}}}$$
$$+ k_{Cyc,\text{Low }T \text{ High SOC}}(T_{\text{Cell}}, I_{\text{Ch}}, SOC) \cdot Q_{\text{Ch}} \quad [2]$$

Model parametrization and validation were conducted through extensive testing featuring various calendar and cycle tests at temperatures from 0 °C to 55 °C. For further details on the calculation of degradation rates as well as model parametrization, the interested reader is referred to.[4]

Total capacity loss under full cycling.—For the development of the control strategy, the degradation rates calculated in the model are first evaluated through parameter sweeps of the degradation model.

The relative total capacity loss per full cycle (Full Equivalent Cycle, FEC) $q_{\text{Loss Total,FEC}}$ is chosen as the loss metric for evaluation of full-cycle operation. The total capacity loss here refers to both calendar as well as cycle degradation. A full cycle consists of a full charge to $SOC = 100\%$ and a full discharge to $SOC = 0\%$ of the battery. The metric is evaluated by calculation of the number of full cycles achievable before the total capacity loss reaches 20% of nominal capacity. The limit is equal to the common End of Life (EOL) criteria of 80% State of Health:[51,65]

$$q_{\text{Loss Total,FEC}} = \frac{Q_{\text{Loss}} = 20\%}{\text{No. of FEC until EOL}} = f(T_{\text{Cell}}, SOC, I_{\text{Ch}}) \quad [3]$$

For the analysis, the battery current, SOC, and cell temperature are set as fixed constant values for both charging and discharging. This makes the evaluation generic, being free of self-heating and heating/cooling effects, and power limitations related to variable cell resistance. Further parameters needed for the model-based evaluation are the Depth of Discharge and the average SOC, which are set at 100% and 50%, respectively.

Figure 2 shows the results for the relative capacity loss per cycle vs (a) cell temperature and (b) vs battery cycling current. Battery current values in all figures in this work are given normalized to the battery nominal capacity as C-Rate. E.g. a C-rate of 1 C charges/discharges a battery's nominal capacity within one hour; 0.5 C within two hours etc.

Results vs cell temperature (Fig. 2a) show that temperature has a strong impact on the total capacity loss per cycle, as expected due to the correlation with degradation in both calendar and cycle ageing. High and low temperatures increase capacity loss compared to a minimum at an optimal temperature. Comparing different battery currents vs temperature shows a different optimum temperature for each specific battery current. Optimum temperature is a combined minimization of the different degradation mechanisms which feature contrary temperature dependencies, e.g. SEI growth and lithium plating

These results illustrate that maintaining a constant operating temperature, usually within a small range around 25 °C, is not the optimal solution in terms of degradation, since that value depends on
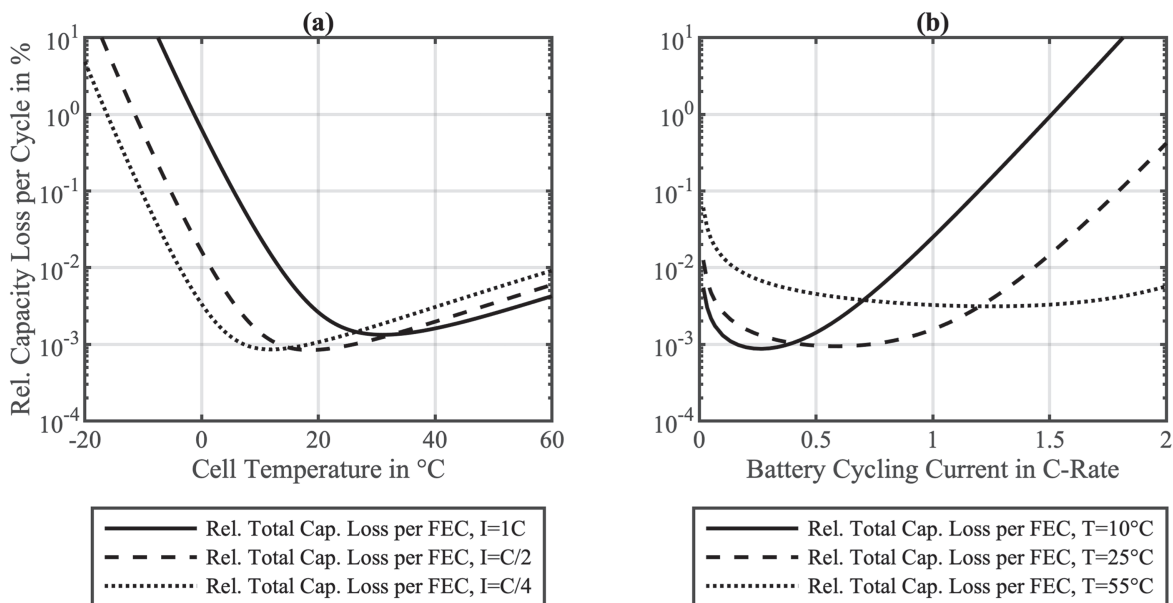

Figure 2. Relative total capacity loss per FEC vs (a) cell temperature and (b) battery cycling current.
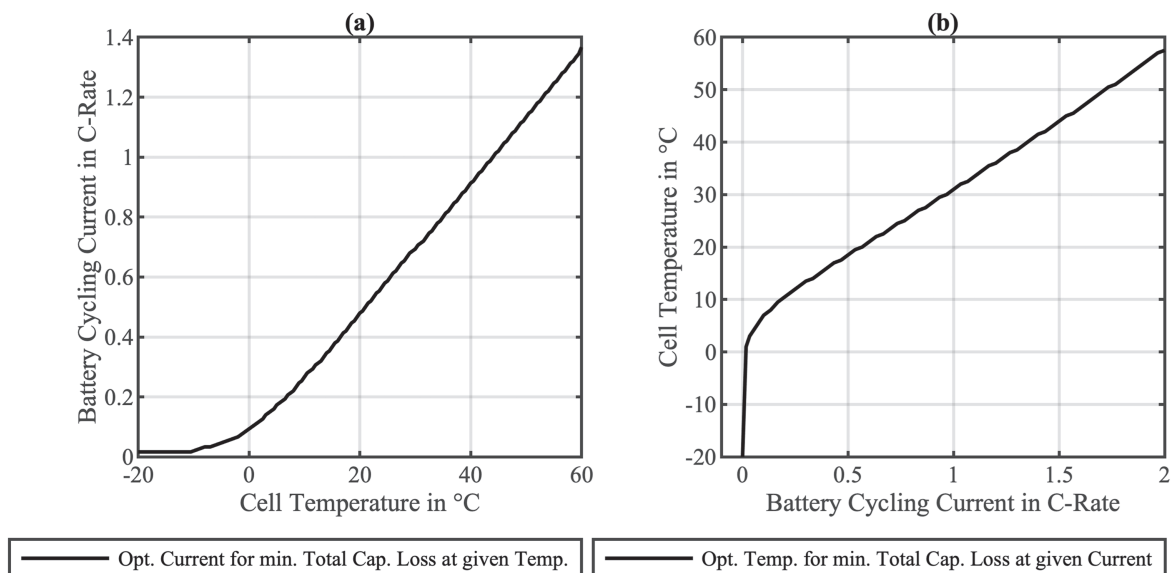
Figure 3. Optimum regarding total capacity loss: (a) Optimal battery cycling current at given temperature and (b) at optimal temperature at given battery cycling current.

the battery current. Nonetheless, that is still a standard control goal for active thermal management systems.

The optimal range for battery operating temperatures has been determined by Pesaran[66] at 25 °C–40 °C, later again by Pesaran[67] at 15 °C–35 °C, and by Ladrech[68] at 20 °C–30 °C. Such different results not thus not only explainable due to different cell investigated, but also with the varying optima for battery temperature seen in Fig. 2.

Results for the total capacity loss curves vs battery cycling current (Fig. 2b) also show an optimum for the best cycling current rate which shifts with temperature. Low currents lead to an increased capacity loss per cycle, which is here mostly attributed to calendar degradation which occurs independently of cycling but strongly dependent on temperature. Higher currents increase the capacity loss per cycle due to increased cycle ageing. This is attributed to degradation mechanisms at a lower temperature, particularly during charging, which feature a battery-current dependence.

Parameter dependencies at minima of total capacity loss per cycle are evaluated in Fig. 3. Results for the optimum battery current of cycling at a given temperature shown in Fig. 3a reveal that with increasing temperatures, the optimum battery current also increases. This is explained by the reduction of cycle capacity losses during charging at higher temperatures, which thus enables more cycles before the cell reaches EOL.

The optimum temperature for a given battery current is shown in Fig. 3b. The optimum temperature increases with the battery current. It can be seen that the higher battery currents for charging require higher temperatures to reduce cycle capacity losses during charging, i.e. lithium plating.

Evaluations of the capacity loss so far analysed the total capacity loss resulting from both calendar and cycle ageing. However, the two mechanisms are highly complex with partially adverse relationships with respect e.g. to temperature. For the development of a practical derating strategy both mechanisms, calendar and cycle ageing, have to be analysed separately.

It is noted, that the separate analysis is valid for the investigated degradation model which features not path-dependent mechanisms. In the case of path-dependent degradations models, a more complex approach with the inclusion of the degradation history would be necessary.

Calendar ageing-induced battery degradation.—For analysis of the calendar ageing, the capacity loss per hour $q_{\text{Loss Cal},p.h.}$ is chosen

as metric:

$$q_{\text{Loss Cal},p.h.} = f(T_{\text{Cell}}, SOC) \qquad [4]$$

Calendar ageing, occurring during storage under various conditions, is simulated until calendar capacity loss reaches the EOL criteria of 20%. Figure 4 shows the results for calendar capacity loss per hour vs (a) cell temperature and (b) SOC.

Higher temperatures lead to an exponentially increasing rate of degradation which is attributed to the Arrhenius rate-law associated with the growth of the SEI.[4]

Higher SOC values also show increasing levels of degradation. Plateaus of different degradation rates are revealed which relate to the different stages of lithiation in the graphite anode. The plateaus are captured in the degradation model through a Tafel equation-based approach by implementing the anode open-circuit voltage in the calendar degradation stress factor k_{Cal}.[4]

Cycle ageing-induced battery degradation.—Cycle-induced battery degradation, as calculated in the degradation model, is strongly influenced by the direction and magnitude of battery current, the SOC, and battery temperature. The model represents those dependencies through the stress factors $k_{\text{Cyc,Low }T}(T_{\text{Cell}}, I_{\text{Ch}})$, $k_{\text{Cyc,Low T High SOC}}(T_{\text{Cell}}, I_{\text{Ch}}, SOC)$, and $k_{\text{Cyc,High }T}(T_{\text{Cell}})$, as well as through the cycle degradation-driving charge throughput in charge direction Q_{Ch}, and in both current directions Q_{Tot}, respectively.

To analyse and subsequently control the degradation with respect to the current direction, the capacity loss per Half Equivalent Cycle (HEC) is chosen as metric for analysis:

$$q_{\text{Loss Cyc,HEC,Ch.}} = f(T_{\text{Cell}}, SOC, I_{\text{Ch}}) \qquad [5]$$

$$q_{\text{Loss Cyc,HEC,Disch.}} = f(T_{\text{Cell}}) \qquad [6]$$

One full cycle consists of an HEC for discharging and an HEC for charging. Again, the cycle operation is simulated until the capacity loss reaches the EOL criteria of 20%. In this evaluation of specifically cycle degradation, the capacity loss results only from the cycle degradation contributions in the respective current direction, neglecting any cycle degradation in the opposite current direction or any calendar degradation.
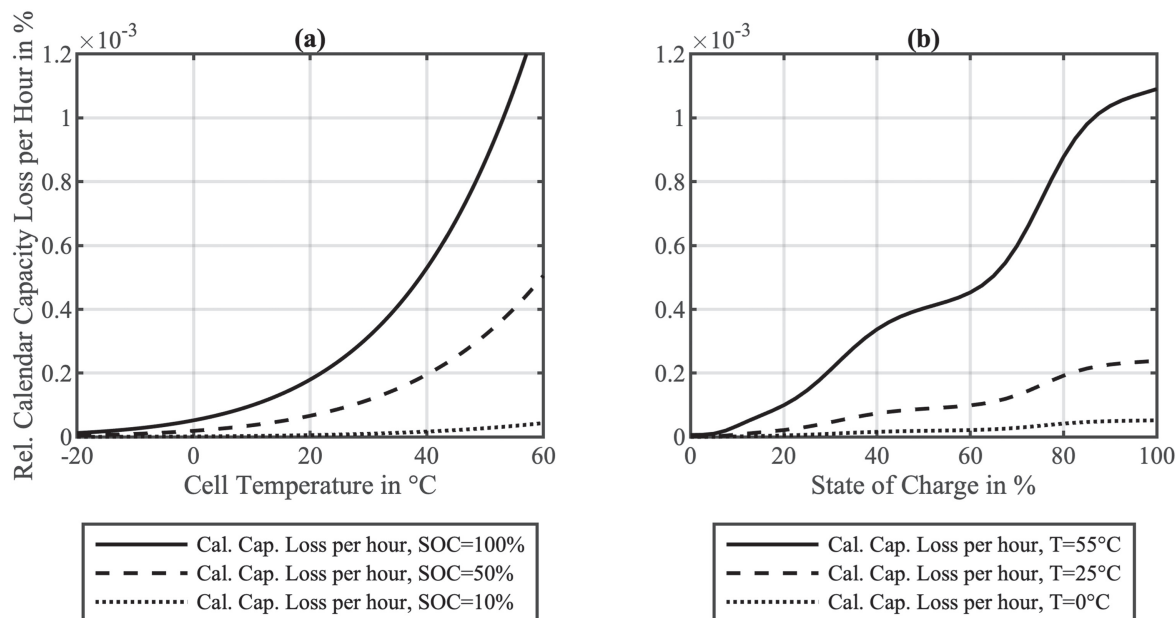
Figure 4. Calendar capacity loss per hour vs (a) cell temperature and (b) SOC.

Figure 5 shows the resulting averaged cycle capacity loss per HEC vs (a) cell temperature and (b) vs battery current.

Evaluating charging/discharging vs temperature in Fig. 5a separately reveals a continuous increase in degradation with higher temperatures for discharging. Instead, for charging, degradation decreases with increasing temperature, from low temperatures towards an optimum, from where on degradation then increases with further increasing temperature. Additionally, for charging, the strong increase in degradation with higher SOC at lower temperatures is shown.

The evaluation of the battery current dependency in Fig. 5b is conducted separately for charging (positive currents) and discharging (negative currents). The calculated cycle degradation for discharging exhibits again only the dependency on temperature, whereas for charging additionally the SOC and battery current both have a strong impact. At the low temperature (0 °C), a strong discontinuity of degradation between discharging and charging is visible, while at the higher temperature (25 °C), this effect is

negligible. The difference is attributed to the reduction of degradation related to lithium plating during charging at low temperatures.

Current-Derating Strategy for Reducing Degradation in Operation

With the previous evaluation in mind, a degradation-aware current-derating strategy can be developed, which employs separate current limits for the reduction of both calendar and cycle degradation. The derating limits for the strategy proposed in this work are developed in section 3.1 and 3.2, respectively, and concluded to a control strategy in section 3.3.

Temperature-based current-derating for calendar ageing reduction.—Typically recommended maximum operating temperatures for Li-ion battery cells range from 30 °C to 60 °C resulting from a consideration of degradation and safety and are in general independent of the SOC. E.g. for the cell chemistry chosen in this
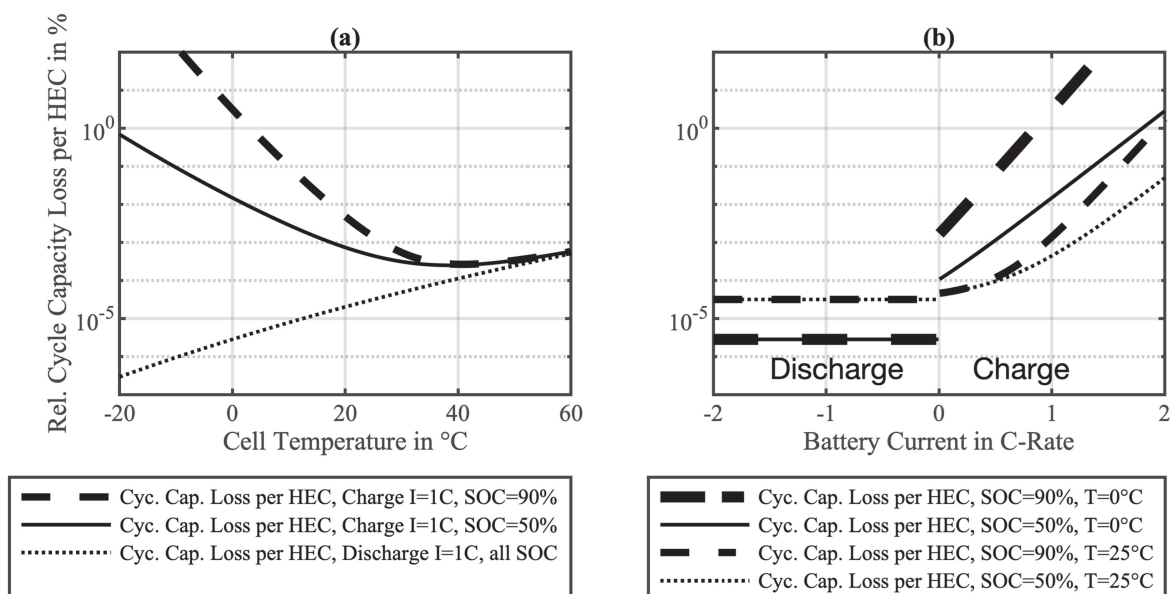

Figure 5. Cycle capacity loss per HEC vs (a) cell temperature and (b) battery current.
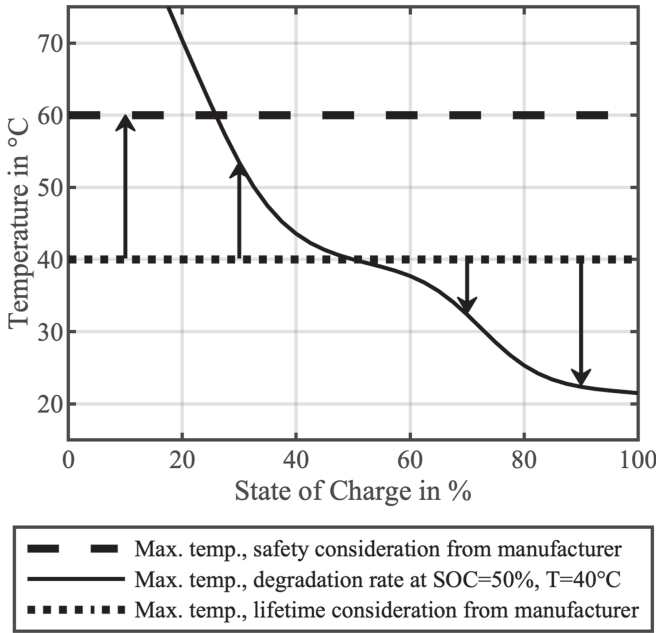
Figure 6. Cell temperature limits based on calendar degradation rate of $T_{\text{Ref,Cal}} = 40$ °C, $SOC_{\text{Ref,Cal}} = 50$ % and safety limit of 60 °C.

work, the manufacturer recommends a maximum cell temperature of 40 °C with a maximum temperature of 60 °C due to battery safety.

Referring to the calendar degradation, however, the degradation model reveals that the rate of calendar ageing is defined by the stress factor, k_{Cal} (Eq. 2), which depends both on T and SOC. Both higher temperature and SOC increase the stress factor.

As the aim of the control strategy is to limit degradation, interdependence can be taken into account. A more advanced rule for determining the maximum cell temperature is proposed, which is not a constant value, but is dependent on the actual SOC.

Therefore, a maximum acceptable stress factor can be defined, which then results in different maximum temperature values. In case the SOC is low, a higher temperature is acceptable, with additional consideration of safety limits. For higher values of SOC, a lower temperature is advised to reduce the rate of degradation.

The maximum cell temperature is calculated depending on the SOC together with a defined maximum acceptable calendar stress factor, e.g. at reference conditions of $T_{\text{Ref,Cal}} = 40$ °C, $SOC_{\text{Ref,Cal}} = 50$ %.

With those defined, the maximum calendar stress factor at reference conditions $q_{\text{Loss Cal},p.h.,\text{Ref}}$ can be calculated to 2.0 e–4% of nominal cell capacity per hour:

$$q_{\text{Loss Cal},p.h.,\text{Ref}} = f(T_{\text{Ref,Cal}}, SOC_{\text{Ref,Cal}}) \qquad [7]$$

For orientation of the values of relative calendar capacity loss per hour, it is referred to Fig. 5.

During operation, with the SOC as an input parameter, the maximum temperature can then be calculated:

$$T_{\text{Max,Degr,Cal}} = f(SOC, q_{\text{Loss Cal},p.h.,\text{Ref}}) \qquad [8]$$

To limit the rate of degradation to the rate at reference conditions, changes in the SOC then lead to changes for the maximum cell temperature. Figure 6 shows the resulting variable maximum cell temperature vs the SOC along with the constant temperature limits from the manufacturer for ageing (40 °C) as well as safety (60 °C). Arrows indicate the SOC-dependent increase as well as decrease of maximum temperature from the recommended constant temperature limits from the manufacturer.

At very low SOC the maximum battery temperature is limited by the safety limits. With increasing SOC, the temperature limit is

continuously reduced and even drops below the standard recommended temperature.

The variable maximum cell temperature is converted into a current-derating strategy by derating the current request to prevent self-heating of the cell above the calculated maximum cell temperature.

For calculation of the maximum current, an electrical-thermal battery model is used, which is in this work an equivalent circuit model calculating overvoltages with a single resistance. The cell resistance R_{Cell} is first calculated from look-up tables, which are implemented as a function of the current direction $\text{sgn}(I_{\text{Req}})$, cell temperature and SOC. Resistance for charging/discharge operation is denoted $+/-$.

$$R_{\text{Cell}}^{+/-} = f(T_{\text{Cell}}, SOC, \text{sgn}(I_{\text{Req}})) \qquad [9]$$

The maximum current $I_{\text{Max,Degr,Cal}}^{+/-}$ is then be calculated by evaluating the maximum cell-internal losses together with the ambient temperature around the cell T_{Ambient}:

$$I_{\text{Max,Degr,Cal}}^{+/-} = f(R_{\text{Cell}}^{+/-}, T_{\text{Cell}}, T_{\text{Ambient}}, T_{\text{Max,Degr,Cal}}) \qquad [10]$$

Figure 7 shows the schematics of the temperature-based current derating for calendar ageing reduction, exemplarily for charging.

At the beginning of the example, the cell temperature starts well below the maximum temperature limit. The current of the cell stays constant, is not derated, and follows the current request. However, with further charging, the SOC increases, resulting in a decreased temperature limit. Additionally, the cell temperature increases due to self-heating. The cell temperature reaches the maximum temperature limit, and from then on, the current is derated and the cell temperature follows the temperature limit.

Current-derating for cycle ageing reduction.—Current derating for cycle ageing reduction is be directly calculated from the degradation model. First, a maximum cycle relative capacity loss at reference conditions is defined. Together with the actual battery state parameters, temperature and SOC, the highest acceptable battery current is then calculated separately for charge/discharge.

Figure 8 shows the results for maximum current vs cell temperature for (a) charging and (b) discharging. The maximum relative cycle capacity loss per HEC applied is calculated exemplarily from reference conditions $T_{\text{Ref,Cyc}} = 40$ °C, $SOC_{\text{Ref,Cyc}} = 50$ %, $I_{\text{Ref,Cyc}} = +1C$ (Charge) to 2.5 e–4% of nominal cell capacity per HEC:

$$q_{\text{Loss Cyc,HEC,Ref.}} = f(T_{\text{Ref,Cyc}}, SOC_{\text{Ref,Cyc}}, I_{\text{Ref,Cyc}}) \qquad [11]$$

For orientation of the values of relative cycle capacity loss per HEC, it is referred to Fig. 5.

Maximum charge current in Fig. 8a is calculated with as a function of SOC and temperature, with $q_{\text{Loss Cyc,HEC,Ref.}}$ defining the maximum rate of cycle degradation:

$$I_{\text{Max,Degr,Cyc}}^{+} = f(T_{\text{Cell}}, SOC, q_{\text{Loss Cyc,HEC,Ref.}}) \qquad [12]$$

The strong correlation of degradation with battery current is again revealed, with the maximum battery current reduced by several orders of magnitude with lower temperatures.

The maximum discharge current calculation features no SOC dependence or correlation with the battery current and is thus only dependent on cell temperature and maximum rate of cycle degradation $q_{\text{Loss Cyc,HEC,Ref.}}$:

$$I_{\text{Max,Degr,Cyc}}^{-} = f(T_{\text{Cell}}, q_{\text{Loss Cyc,HEC,Ref.}}) \qquad [13]$$

The resulting maximum battery discharge current shown in Fig. 8b is therefore a step function that allows discharge operation up to a specific temperature.
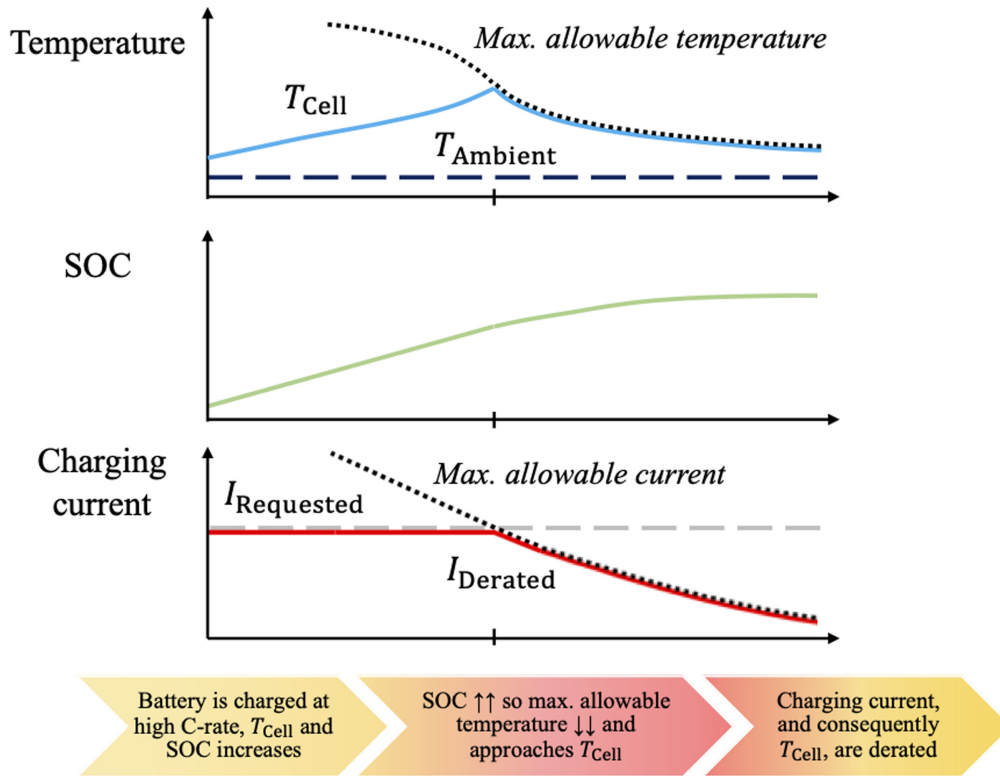
Figure 7. Temperature-based current derating for calendar ageing reduction, example for charging.

The maximum current for charge/discharge is then directly used for current derating. For visualization, Fig. 9 shows the schematics of the current derating for cycle ageing reduction, exemplarily for charging.

In this example case, the cell temperature starts with low values, leading to low current values for the cycle-degradation current limit. The battery current request is derated to the current limit. With ongoing charge operation, the battery temperature increases and leads to increasing cycle ageing current limits. Finally, with further increased battery temperatures, the cycle ageing current limit is higher than the current request to the battery and therefore does not derate the battery current request anymore.

Summary of the current-derating control strategy.—Figure 10 shows the integration of both calendar and cycle ageing current-derating strategies into a battery system model or a battery control system.

The system simulation or the battery management system provides the required battery cell and system parameters. Cell parameters are in this case SOC and T_{Cell}. Required system parameters are the ambient
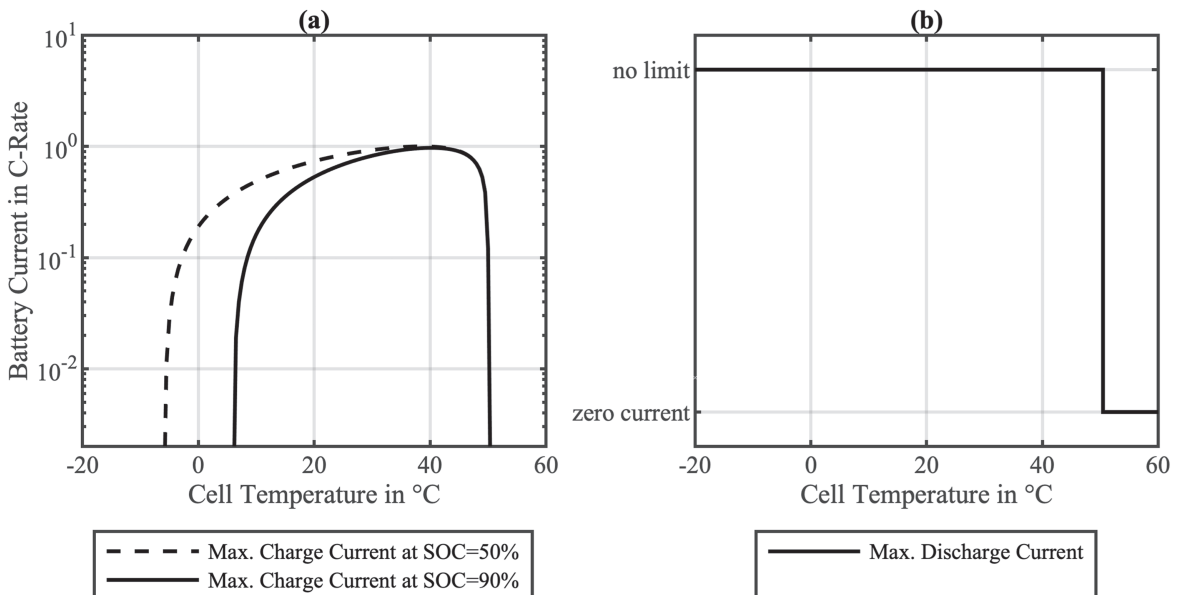

Figure 8. Maximum battery current vs cell temperature for (a) charging and (b) discharging, based on maximum relative cycle capacity loss of 2.5 e–4% per HEC, calculated from reference conditions $T_{Ref,Cyc} = 40°C$, $SOC_{Ref,Cyc} = 50\%$, $I_{Ref,Cyc} = +1C$ (Charge).
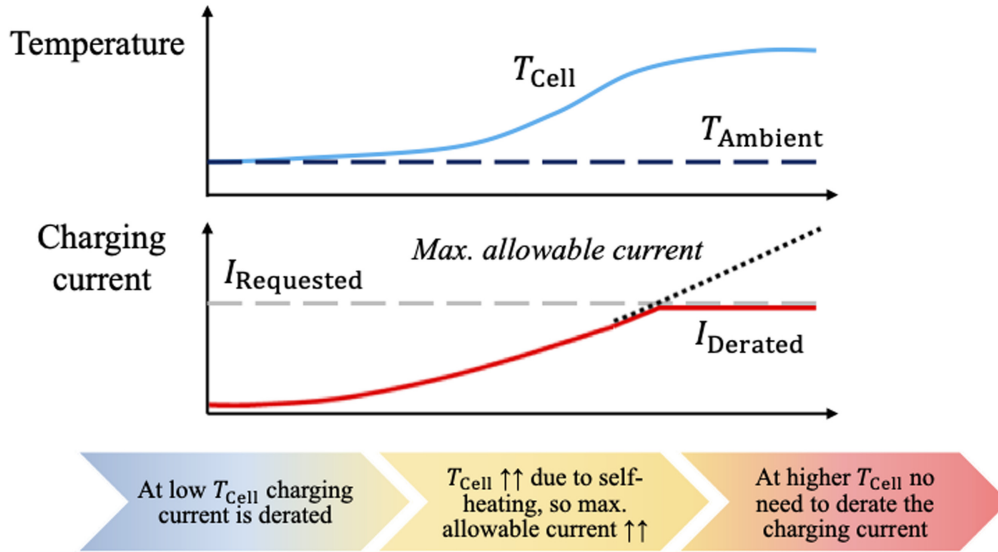
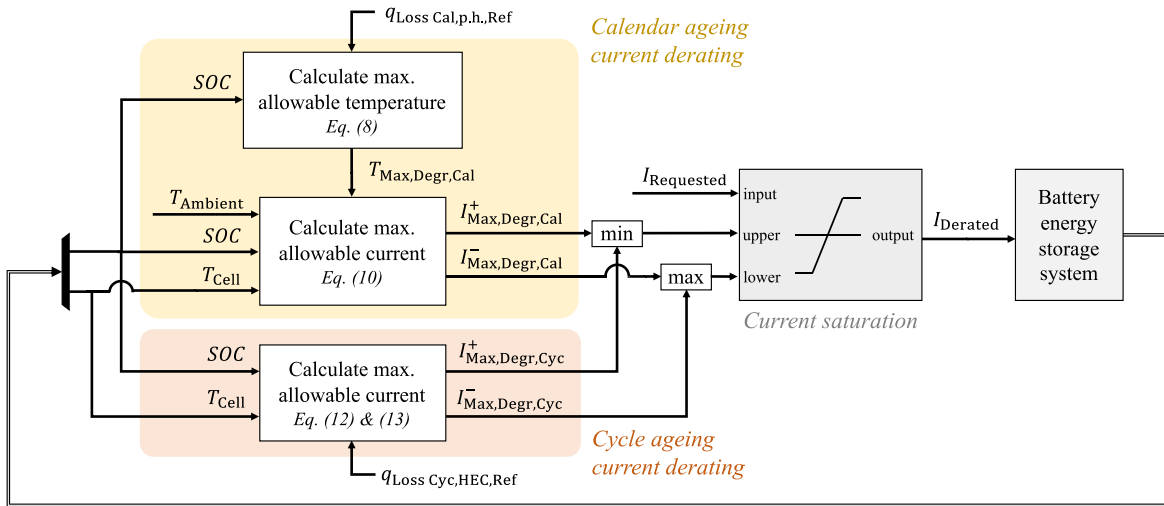**Figure 9.** Schematics of current derating for cycle ageing reduction, example for charging.

Figure 10. Integration of novel degradation-aware current derating in system simulation/control.

temperature to cell for thermal calculations T_{Ambient}, as well as the current request to the battery I_{Req} to the derating strategy.

With the variable inputs, the maximum rates for the respective degradation mechanisms defined through reference conditions, and the electrical-thermal cell model the calculations for current derating are then performed.

For calendar ageing reduction, first the maximum temperature $T_{\text{Max,Degr,Cal}}$ is calculated from the cell SOC with respect to the degradation at reference conditions $q_{\text{Loss Cal},p.h.,\text{Ref}}$. Additionally, safety limits for temperature are respected. Then, the maximum battery current for calendar ageing reduction $I_{\text{Max,Degr,Cal}}^{+/-}$ is calculated from the electrical-thermal model with cell temperature T_{Cell}, ambient temperature T_{Ambient}, and SOC such as that cell temperature will not increase above $T_{\text{Max,Degr,Cal}}$.

For cycle ageing reduction, the degradation model directly calculates the maximum current $I_{\text{Max,Degr,Cyc}}^{+/-}$ from cell temperature T_{Cell}, and SOC with respect to the rate of degradation at reference conditions $q_{\text{Loss Cyc,HEC,Ref}}$.

Finally, the derated current I_{Derated} is calculated as the minimum from the current request and maximum battery currents for ageing

reduction. The derated current is then given as input to the system simulation or system control. Other standard current-derating processes such as cell voltage limits are performed afterwards.

Application of Current-Derating Strategy in Residential PV Buffer BESS

The developed current-derating control strategy is evaluated in a system simulation of a stationary BESS.

Scenario summary.—The BESS is simulated in an application as a residential PV buffer system. In this scenario, the battery charges excess power from the PV system when the PV power production exceeds the household consumption and discharges when the household consumption cannot be supplied fully directly from the PV system. Figure 11 shows the schematics of the system structure with an AC-coupled battery.

The household load profile is taken as the Standard Load Profile *H0* for German households with a temporal resolution of 1 h and scaled to a yearly consumption of 5,000 kWh/a.[69]

The PV system is sized to 10 kW peak power. The time-power-profile is calculated with a 15 min temporal resolution using the
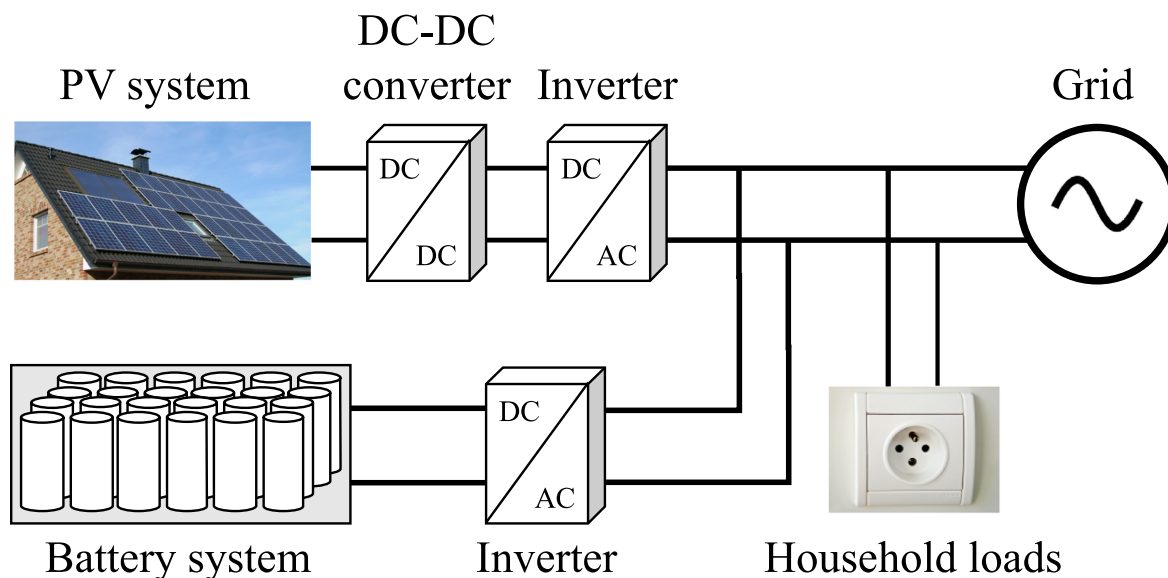
Figure 11. System topology schematic of an AC-coupled BESS in a residential PV energy system.

software Greenius 4.1.1 by the German Aerospace Center (DLR).[70] Meteorological data for PV power production is set to Berlin, Germany.

In accordance with the household load profile being representative for Germany and the meteorological input data for the simulation of PV power being set to Berlin, the ambient outdoor conditions for the thermal battery system simulation are set for an outdoor application in Berlin, Germany. The time-ambient temperature-profile with a 1 h temporal resolution is also taken from the software Greenius.[70] Temperature profile values for the data are min. –14.6 °C, mean + 8.9 °C, and max. +31.4 °C.

The BESS is parametrized with a nominal energy of 2.5 kWh. Thermal management of the battery system is simulated as a passively-cooled closed system, meaning no active heating/ventilation/cooling of the system is performed. The degradation-aware derating strategy improves system operation especially under unfavourable operating conditions, which are expected with passive-cooled systems in an outdoor installation. Awadallah presented grid pole-mounted BESS with a small capacity.[71] For such small outdoor-installed systems, a dedicated active thermal management system is especially cost-prohibitive.

To focus on the aspects of battery control, power electronics and their limits or losses are not included in the simulation. Furthermore, possible system-internal thermal gradients are excluded from the evaluation. The system-internal air is calculated as ideally-mixed, and the battery cells are simulated using a single-cell model. The system power request is calculated first and then scaled down to the single-cell level for coupling of system operation and cell simulation.

The electrical equivalent-circuit model, as well as the 0D-thermal-cell model, are both parametrized for the same SONY lithium iron phosphate/graphite cell used in the parametrization of the battery degradation model. For further details on the electrical-thermal cell model, it is referred to.[37]

Figure 12 shows the thermal model for the battery system. Heat transfer between ambient outdoor air, system steel casing, system-internal air, and finally to the battery cell is calculated as convective heat transfer. System geometry is calculated as a cube geometry with the system volume corresponding to the number of cells enclosed with a packing efficiency of 75%, leaving 25% of the volume for air.

For further details on the thermal system model, which is based on building simulation parameters used here, it is here referred to.[37]

Operation is simulated for a full year to cover seasonal variations of PV power, household load, and ambient conditions. Battery
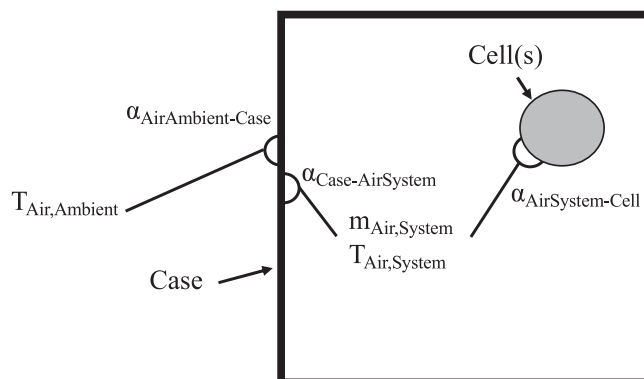

Figure 12. Thermal system model with a single cell model and ideally-mixed system-internal air.

degradation from the second year onwards is extrapolated from the first fully simulated year until EOL at a capacity of 80%. Energy throughput is calculated with a linearly-reduced value for each year according to the respective cell capacity in each year.

Application results.—Parameters for the current derating are set as in the previously shown evaluations (Fig. 6, Fig. 8) to reference conditions of $T = 40$ °C and $SOC = 50$ % for both calendar and cycle degradation and additionally a battery current of $+1$ C for cycle degradation.

For a detailed evaluation of the current-derating strategy, different parts of the derating strategy are activated and simulated individually, namely calendar and cycle degradation reduction separately, as well as derating activated only during charging and discharging—resulting in four separate scenarios. Additionally, a scenario with the complete control strategy consisting of all four derating modes applied is evaluated (Scenario *All Degr. Limits*).

For reference, a simulation with no current derating (scenario *No Limit*) is performed, as well as a simulation with simple current derating according to manufacturer SOA specifications (scenario *Manufact. Limit*), with constant current limits for charge 1 C, discharge 2 C, and temperature window for operation between -20 °C and $+60$ °C.

In all scenarios, the limits for cell voltage (2.0 V to 3.6 V) and SOC (0% to 100%) specified by the manufacturer are respected.

Figure 13 shows the results for all seven simulated scenarios. To evaluate the impact of the control strategy on the performance of the system, the energy output of the battery in its first year is shown in Fig. 13a. To analyse the reduction of battery degradation, the lifetime of the battery in each scenario is shown in Fig. 13b. Finally, to evaluate the lifetime performance, the combination of the two first results, the energy output over battery lifetime until EOL is shown in Fig. 13c.

As the battery system parameters, as well as the reference conditions of the applied current-derating strategies, are only exemplary, the relative values calculated normalized to the scenario *No Limit* are shown. Absolute values are not shown as simulation results e.g. the absolute lifetime of the battery system is dependent on study parameters such as battery size, which are however not the focus of this study.

The evaluation of the energy output in the first year (Fig. 13a) shows that the degradation-aware derating active during charging operation in the Scenarios *Cyc. Degr. Ch. Limit* and *Cal. Degr. Ch. Limit* have a big effect on operation. In the scenario *Cyc. Degr. Disch. Limit* no actual limiting occurs, as cell temperature does not

reach the relevant temperature level. In scenario *Cal. Degr. Disch. Limit* operation limiting occurs rarely and thus energy output is only negligibly changed. Scenario *All Degr. Limits* shows the strongest reduction in energy output. Scenario *Manufacturer Limit* instead even shows a slight increase in energy output due to reduced ageing in the first year while only negligibly limiting battery current.

Evaluation of the battery lifetime (Fig. 13b) shows a strong increase in battery lifetime for the scenarios *Cyc. Degr. Ch. Limit* and *Cal. Degr. Ch. Limit*, which previously also impacted operation the strongest. Scenario *Cal. Degr. Disch. Limit* even shows a slightly negative impact on battery lifetime, which can be explained as the limiting of the discharge current during high temperatures can lead to a longer duration at high SOC and high temperature. Similar to the energy throughput evaluation, scenario *All Degr. Limits* shows the strongest change due to the combination of all degradation-reducing current limits.

For scenario *All Degr. Limits,* comparing the relative changes for reduction of energy output to the increases in battery lifetime signals a possible positive outcome for the energy output over battery lifetime until EOL (c). The combined scenario *All Degr. Limits*
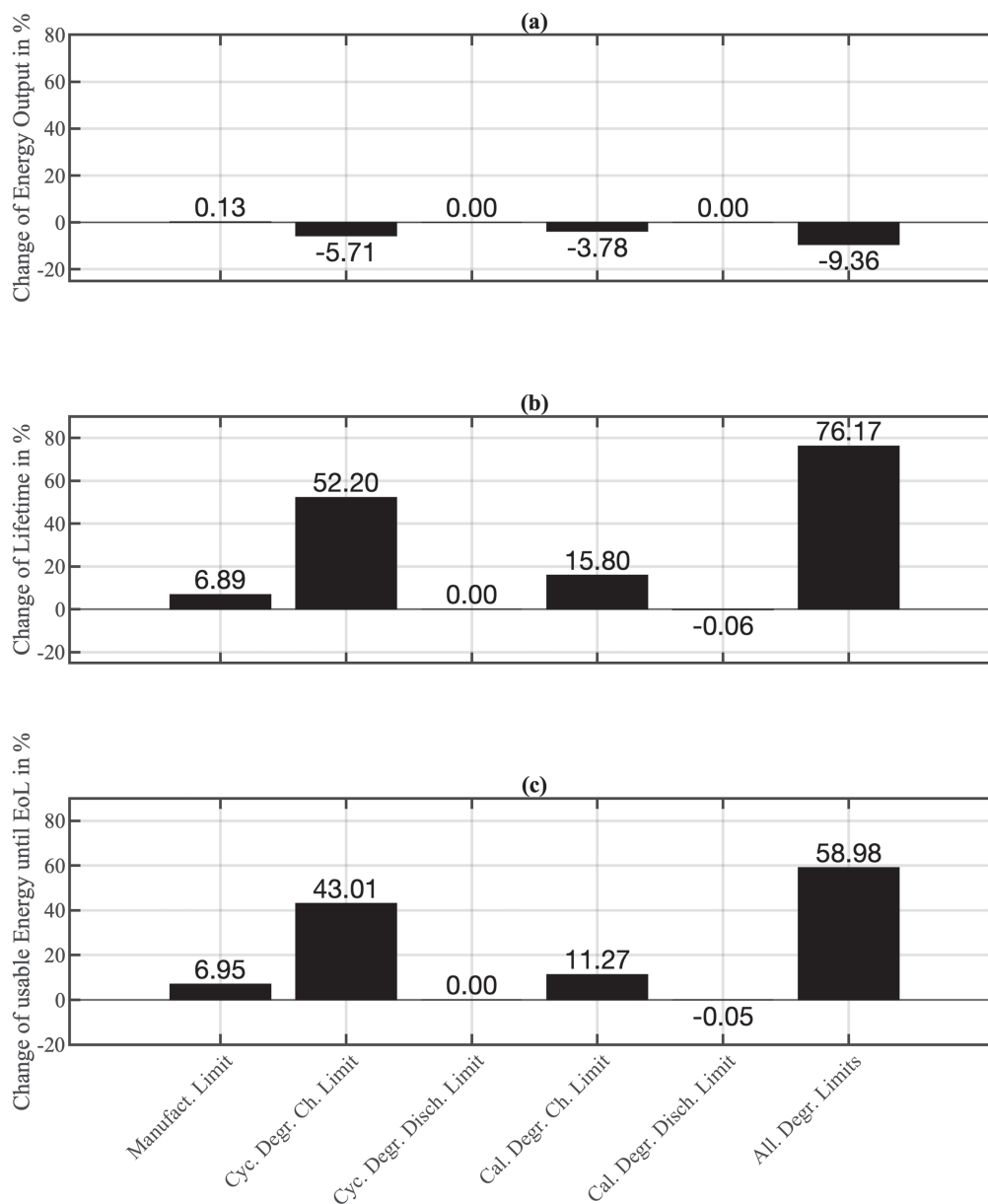

Figure 13. Comparison of derating strategies: (a) energy output in year one, (b) battery lifetime, (c) energy throughput until EOL. All results normalized to *No Limit* scenario.
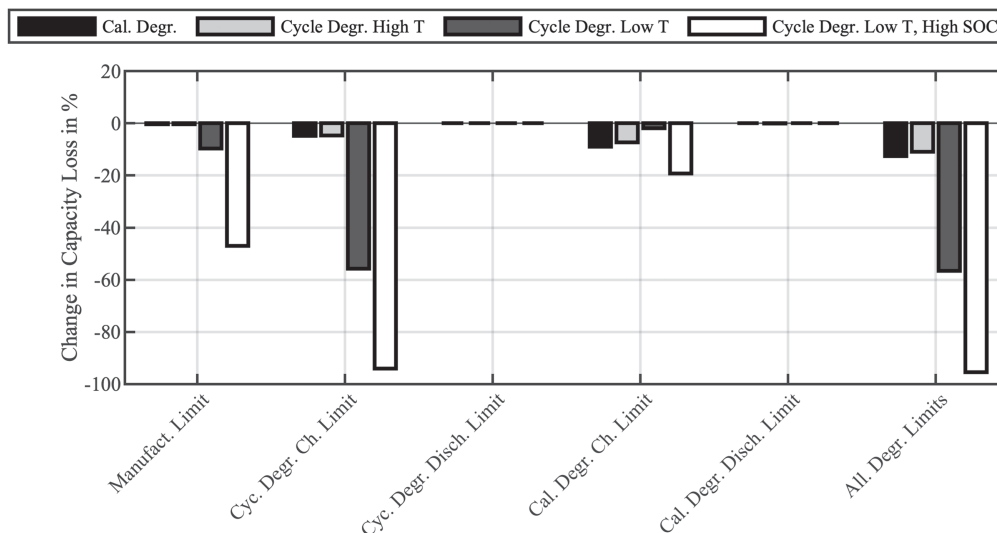
Figure 14. Impact of derating on degradation mechanisms. All results normalized to *No Limit* scenario.

shows a significant increase in energy output over the battery lifetime.

Putting the results of the combined scenario *All Degr. Limits* into the second reference of the scenario *Manufacturer Limit* reveals an increase of battery lifetime by 65%, an increase in energy throughput over lifetime by 49%, while system energy throughput per year is reduced by only 9%. The degradation-aware operation thus also outperforms the operation according to manufacturer specifications.

To analyse the reduction in capacity losses in the respective loss mechanisms in detail, Fig. 14 shows the change of each mechanism, again normalized to the Scenario *No Limit*.

Calendar degradation shows a strong reduction in the Scenario *Cal. Degr. Ch. Limit,* but also in the Scenario *Cyc. Degr. Ch. Limit*, where a reduction in charging current leads to reduced temperatures as well as reduced/delayed increases in SOC.

Breaking down cycle degradation into its three sub-mechanisms reveals a significant reduction of cycle degradation at low temperatures. Cycle degradation related to high temperatures is reduced significantly less. Finally, the Scenario *All Degr. Limits* shows a reduction for all four loss mechanisms.

Sensitivity analysis of the maximum degradation rate.—The scenario simulations evaluated so far in section 4.2 considered exemplary degradation rate limits that were not optimized for a specific application. A sensitivity analysis for tuning the degradation rate limits, for both calendar and cycle degradation, is shown in Fig. 15.

In the sensitivity analysis for calendar/cycle ageing reduction, derating for reducing either calendar or cycle ageing is analysed separately. I.e. in the sensitivity analysis of calendar ageing reduction, no derating for cycle ageing reduction is applied.

The change of the analysed degradation rate relative to the degradation rate at reference conditions is shown on the *x*-axis. The change of the respective results relative to the results at reference conditions (Scenario *No Limit*) is shown on the *y*-axis.

Evaluating the sensitivity of calendar ageing with respect to changes in the maximum degradation rate reveals an increase of the maximum rate by 100%, a complete elimination of the derating effect. Decreasing the maximum degradation rate significantly reduces the energy output of the system, leading to an increased lifetime as well as lifetime energy throughput. However, a turning point is revealed with further reduced maximum degradation rates. The system is barely operating due to the derating, leading to very low energy output. The resulting lifetime increase does not outweigh the effect and the lifetime energy throughput is also significantly decreased.

The sensitivity analysis of cycle ageing reduction shows similar results, except for more stable improvements of lifetime as well as lifetime energy throughput at higher maximum degradation rates.

Conclusion and Outlook

Currently, the standard strategies for derating and thermal management do not account for the complexity of battery degradation mechanisms. This may be seen as a simplistic solution to a complex problem. To tackle this, other authors have proposed the online integration of degradation models and optimization strategies in the derating strategy, particularly to manage the charging process. The problem is that this may be seen as partial and complex solutions to a complex problem, limiting widespread adoption. In contrast, here we use the degradation model offline to predetermine the degradation rates through parameter sweeps. Then, these results are integrated into the derating control. This framework can be adapted to any degradation model, and allows flexible tuning of the algorithm, which can be more or less restrictive.

A simulation-based evaluation of the control strategy in a stationary BESS showed a strong impact on system operation. By derating the current and therefore reducing the operation at unfavourable conditions, the energy output was reduced by only single digits, whereas the battery lifetime, as well as the energy output over lifetime until EOL, both increased strongly in the high double-digit range. Battery lifetime was almost increased by a factor of two.

The current-derating strategy is directly usable in applications where the control of battery power is with the system operator and not controlled externally. For stationary grid-coupled applications, this results in applicability e.g. for PV buffer or energy trading but not for control reserve provision such as frequency control where system power is set through regulation and offers little flexibility.

We show that the control strategy can be tuned for different goals, e.g. short, more intensive system operation or longer, less intensive operation.

Future work on the derating strategy can improve the optimal determination of the maximum degradation rate. Replacing the constant values with online calculation could further improve operational results.

E.g., during simulation/operation the parameters could be adapted e.g. monthly to align battery lifetime with the desired goals. A second possibility is to calculate the maximum degradation rate individually based on the current situation, e.g. achievable revenue/profit in energy trading applications. Finally, using forecast or
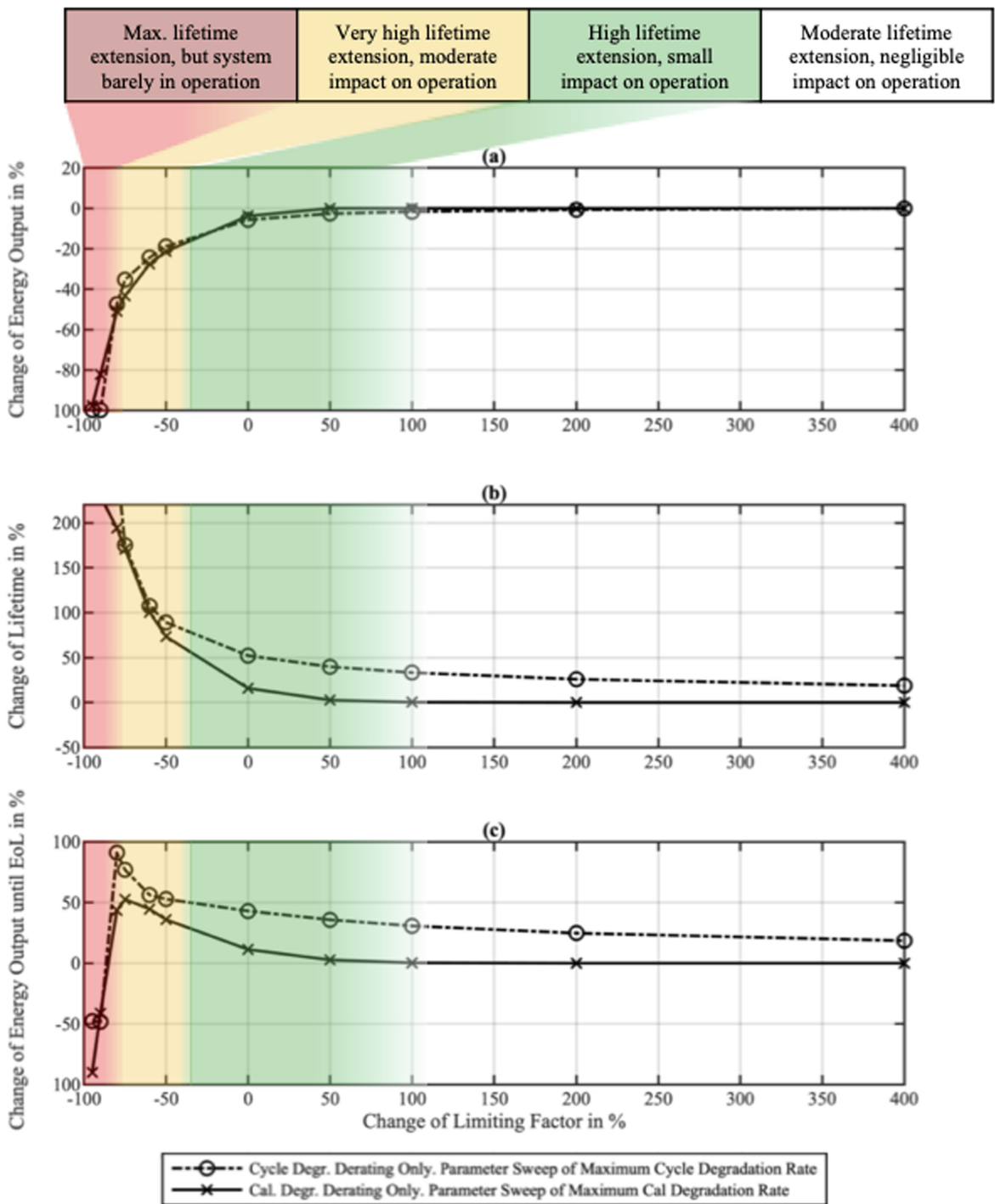
Figure 15. Sensitivity analysis for degradation rate limits: (a) energy output in year one, (b) battery lifetime, (c) energy throughput until EOL. All results normalized to *No Limit* scenario.

historical data, the maximum degradation rate could also be optimized to achieve maximum energy throughput until EoL.

Future application studies should evaluate the economics of prolonging the battery lifetime, as e.g. in grid storage systems, the revenue is reduced in the short term but increased in the long term. An economic evaluation considering a discount factor could reveal an optimum between short- and long-term revenues.

The derating algorithm can also be assessed in other applications of Li-ion cells besides grid storage systems, and in combination with advanced balancing systems, evaluating the impact on cell-to-cell variations too.

ORCID

Michael Schimpe https://orcid.org/0000-0001-5000-2045
Jorge V. Barreras https://orcid.org/0000-0003-2791-1368
Billy Wu https://orcid.org/0000-0003-3963-4900
Gregory J. Offer https://orcid.org/0000-0003-1324-8366

References

1. H. Hesse, M. Schimpe, D. Kucevic, and A. Jossen, *Energies*, **10**, 2107 (2017).
2. M. Naumann, M. Schimpe, P. Keil, H. C. Hesse, and A. Jossen, *Journal of Energy Storage*, **17**, 153 (2018).
3. M. Schimpe, M. E. von Kuepach, M. Naumann, H. C. Hesse, A. Jossen, K. Smith, and S. Santhanagopalan, *ECS Meeting Abstracts*, **MA2017-02**, 179 (2017).
4. M. Schimpe, M. E. von Kuepach, M. Naumann, H. C. Hesse, K. Smith, and A. Jossen, *J. Electrochem. Soc.*, **165**, A181 (2018).
5. K. Smith, M. Baggu, A. Friedl, T. Bialek, and M. R. Schimpe, *2017 IEEE Power & Energy Society General Meeting*, Chicago, IL, USA, 16–20 July 2017 (IEEE) p. 1 (2017).
6. J. V. Barreras, T. Raj, and D. A. Howey, *IECON 2018 – 44th Annual Conference of the IEEE Industrial Electronics Society*, Washington, DC, USA, 21–23 Oct. 2018 (IEEE) p. 4956 (2018).
7. Y. Sun, S. Saxena, and M. Pecht, *Energies*, **11**, 3295 (2018).
8. J. Kim, J. Oh, and H. Lee, *Appl. Therm. Eng.*, **149**, 192 (2019).
9. J. Neubauer and E. Wood, *J. Power Sources*, **259**, 262 (2014).
10. K. Smith, A. Saxon, M. Keyser, B. Lundstrom, C. Ziwei, and A. Roc, *2017 American Control Conference (ACC)*, Seattle, WA, USA, 24–26 May 2017 (IEEE) p. 4062 (2017).
11. K. Smith, Y. Shi, and S. Santhanagopalan, *2015 American Control Conference (ACC)*, Chicago, IL, USA, 1–3 July 2015 (IEEE) p. 728 (2015).
12. W. Wu, S. Wang, W. Wu, K. Chen, S. Hong, and Y. Lai, *Energy Convers. Manage.*, **182**, 262 (2019).
13. T. Yuksel, S. Litster, V. Viswanathan, and J. J. Michalek, *J. Power Sources*, **338**, 49 (2017).
14. Z. Rao, S. Wang, M. Wu, Z. Lin, and F. Li, *Energy Convers. Manage.*, **65**, 92 (2013).
15. J. Cao and A. Emadi, *IEEE Trans. Power Electron.*, **27**, 122 (2012).
16. M. Choi, S. Kim, and S. Seo, *IEEE Trans. Smart Grid*, **3**, 463 (2012).
17. F. S. Garcia, A. A. Ferreira, and J. A. Pomilio, *2009 Twenty-Fourth Annual IEEE Applied Power Electronics Conference and Exposition*, Washington, DC, USA, 15–19 Feb. 2009 (IEEE) p. 826 (2009).
18. C. Pinto, J. V. Barreras, R. D. Castro, E. Schaltz, S. J. Andreasen, and R. E. Araujo, *2014 IEEE Vehicle Power and Propulsion Conference (VPPC)*, Coimbra, Portugal, 27–30 Oct. 2014 (IEEE) p. 1 (2014).
19. C. Pinto, J. V. Barreras, R. de Castro, R. E. Araújo, and E. Schaltz, *Energy*, **137**, 272 (2017).
20. Y. Zhang, Z. Jiang, and X. Yu, *2008 IEEE Energy 2030 Conference*, Atlanta, GA, USA, 17–18 Nov. 2008 (IEEE) p. 1 (2008).
21. J. V. Barreras, C. Pinto, R. D. Castro, E. Schaltz, S. J. Andreasen, and R. E. Araujo, *2014 IEEE Vehicle Power and Propulsion Conference (VPPC)*, Coimbra, Portugal, 27–30 Oct. 2014 (IEEE) p. 1 (2014).
22. D. F. Frost and D. A. Howey, *IEEE Trans. Power Electron.*, **33**, 729 (2018).
23. C. Pinto, J. V. Barreras, E. Schaltz, and R. E. Araújo, *IEEE Trans. Sustainable Energy*, **7**, 1703 (2016).
24. A. Pröbstl, S. Park, S. Narayanaswamy, S. Steinhorst, and S. Chakraborty, *2018 Design, Automation & Test in Europe Conference & Exhibition (DATE)*, Dresden, Germany, 19–23 March 2018 (IEEE) p. 431 (2018).
25. M. M. U. Rehman, M. Evzelman, K. Hathaway, R. Zane, G. L. Plett, K. Smith, E. Wood, and D. Maksimovic, *IEEE Energy Conversion Congress and Exposition (ECCE)*, Pittsburgh, PA, USA, 14–18 Sept. 2014 (IEEE) p. 4327 (2014).
26. Y. Shi, K. Smith, R. Zane, and D. Anderson, *2017 American Control Conference (ACC)*, Seattle, WA, USA, 24–26 May 2017 (IEEE) p. 4704 (2017).
27. R. Klein, N. A. Chaturvedi, J. Christensen, J. Ahmed, R. Findeisen, and A. Kojic, *Proceedings of the 2011 American Control Conference*, San Francisco, CA, USA, 29 June–1 July 2011 (IEEE) p. 382 (2011).
28. Y. Gao, J. Jiang, C. Zhang, W. Zhang, Z. Ma, and Y. Jiang, *J. Power Sources*, **356**, 103 (2017).
29. U. R. Koleti, C. Zhang, R. Malik, T. Q. Dinh, and J. Marco, *Journal of Energy Storage*, **24**, 100798 (2019).
30. Y. Yin, Y. Bi, Y. Hu, and S.-Y. Choe, *J. Electrochem. Soc.*, **167**, 160559 (2021).
31. K. Sahu (2008), NASA/TP-2003–212242 Instructions for EEE parts selection, screening, qualification, and derating, https://nepp.nasa.gov/docuploads/FFB52B88-36AE-4378-A05B2C084B5EE2CC/EEE-INST-002_add1.pdf.
32. IEEE SA, (2016), Recommended Practice for Maintenance, Testing, and Replacement of Valve-Regulated Lead-Acid Batteries for Stationary Applications (IEEE 1188), https://standards.ieee.org/project/1188.html.
33. NXP (2018), Freescale Semiconductor Data, MPC7447AECS01AD Specification, https://www.nxp.com/docs/en/data-sheet/MPC7447AECS01AD.pdf.
34. Hitachi, Instructions for Use of Hitachi High-Voltage Monolithic ICs, https://www.hitachi-power-semiconductor-device.co.jp/en/products/ic/pdf/Instructions_for_Use_EN.pdf.
35. J. Sowe, S. Few, J. Varela Barreras, M. Schimpe, B. Wu, J. Nelson, and C. Candelise, *ECS Meeting Abstracts*, **MA2020–02**, 3780 (2020).
36. T. Waldmann, M. Wilka, M. Kasper, M. Fleischhammer, and M. Wohlfahrt-Mehrens, *J. Power Sources*, **262**, 129 (2014).
37. M. Schimpe, M. Naumann, N. Truong, H. C. Hesse, S. Santhanagopalan, A. Saxon, and A. Jossen, *Appl. Energy*, **210**, 211 (2018).
38. M.-K. Tran and M. Fowler, *Algorithms*, **13**, 62 (2020).
39. L. B. Diaz, X. He, Z. Hu, F. Restuccia, M. Marinescu, J. V. Barreras, Y. Patel, G. Offer, and G. Rein, *J. Electrochem. Soc.*, **167**, 090559 (2020).
40. V. A. Kharchenko, *Modern Electronic Materials*, **1**, 88 (2015).
41. C. Patsios, B. Wu, E. Chatzinikolaou, D. J. Rogers, N. Wade, N. P. Brandon, and P. Taylor, *Journal of Energy Storage*, **5**, 48 (2016).
42. C. Delacourt and M. Safari, *J. Electrochem. Soc.*, **159**, A1283 (2012).
43. X. Jin, A. Vora, V. Hoshing, T. Saha, G. Shaver, R. E. García, O. Wasynczuk, and S. Varigonda, *J. Power Sources*, **342**, 750 (2017).
44. J. M. Reniers, G. Mulder, and D. A. Howey, *J. Electrochem. Soc.*, **166**, A3189 (2019).
45. S. Grolleau, A. Delaille, H. Gualous, P. Gyan, R. Revel, J. Bernard, E. Redondo-Iglesias, and J. Peter, *J. Power Sources*, **255**, 450 (2014).
46. E. Sarasketa-Zabala, I. Gandiaga, L. M. Rodriguez-Martinez, and I. Villarreal, *J. Power Sources*, **272**, 45 (2014).
47. E. Sarasketa-Zabala, I. Gandiaga, E. Martinez-Laserna, L. M. Rodriguez-Martinez, and I. Villarreal, *J. Power Sources*, **275**, 573 (2015).
48. M. Naumann, F. B. Spingler, and A. Jossen, *J. Power Sources*, **451**, 227666 (2020).
49. J. Wang, P. Liu, J. Hicks-Garner, E. Sherman, S. Soukiazian, M. Verbrugge, H. Tataria, J. Musser, and P. Finamore, *J. Power Sources*, **196**, 3942 (2011).
50. M. Ecker, J. B. Gerschler, J. Vogel, S. Käbitz, F. Hust, P. Dechent, and D. U. Sauer, *J. Power Sources*, **215**, 248 (2012).
51. J. Schmalstieg, S. Käbitz, M. Ecker, and D. U. Sauer, *J. Power Sources*, **257**, 325 (2014).
52. M. Swierczynski, D. Stroe, A. Stan, R. Teodorescu, and S. K. Kær, *IEEE Trans. Ind. Appl.*, **51**, 3453 (2015).
53. E. Sarasketa-Zabala, E. Martinez-Laserna, M. Berecibar, I. Gandiaga, L. M. Rodriguez-Martinez, and I. Villarreal, *Appl. Energy*, **162**, 839 (2016).
54. M. Schimpe, M. Edler von Kuepach, M. Naumann, H. C. Hesse, K. Smith, and A. Jossen, *ECS Trans.*, **80**, 147 (2017).
55. P. P. Mishra, A. Latif, M. Emmanuel, Y. Shi, K. McKenna, K. Smith, and A. Nagarajan, *Appl. Energy*, **264**, 114632 (2020).
56. G. Angenendt, S. Zurmühlen, H. Axelsen, and D. U. Sauer, *Appl. Energy*, **229**, 884 (2018).
57. J. M. Reniers, G. Mulder, S. Ober-Blöbaum, and D. A. Howey, *J. Power Sources*, **379**, 91 (2018).
58. C. Goebel, H. Hesse, M. Schimpe, A. Jossen, and H. Jacobsen, *IEEE Trans. Power Syst.*, **32**, 2724 (2017).
59. V. Kumtepeli, Y. Zhao, M. Naumann, A. Tripathi, Y. Wang, A. Jossen, and H. Hesse, *Int. J. Energy Res.*, **43**, 4127 (2019).
60. M. Schimpe, C. N. Truong, M. Naumann, A. Jossen, H. C. Hesse, J. M. Reniers, and D. A. Howey, *2018 IEEE International Conference on Environment and Electrical Engineering and 2018 IEEE Industrial and Commercial Power Systems Europe (EEEIC / I&CPS Europe)*, Palermo, Italy, 12th to 15th June, 2018, p. 1 (2018).
61. H. Hesse, V. Kumtepeli, M. Schimpe, J. Reniers, D. Howey, A. Tripathi, Y. Wang, and A. Jossen, *Energies*, **12**, 999 (2019).
62. V. Kumtepeli, H. C. Hesse, M. Schimpe, A. Tripathi, Y. Wang, and A. Jossen, *IEEE Access*, **1**, 204325 (2020).
63. M. Schimpe, J. V. Barreras, B. Wu, and G. J. Offer, *ECS Meeting Abstracts*, , **MA2020–02**, 3808 (2020).
64. C. N. Truong, M. Schimpe, M. Naumann, A. Jossen, and H. C. Hesse, *International ETG Congress*, **2017**, 1 (2017), https://ieeexplore.ieee.org/abstract/document/8278767.
65. S. F. Schuster, T. Bach, E. Fleder, J. Müller, M. Brand, G. Sextl, and A. Jossen, *Journal of Energy Storage*, **1**, 44 (2015).
66. A. A. Pesaran, *J. Power Sources*, **110**, 377 (2002).
67. A. Pesaran, M. Keyser, G. Kim, S. Santhanagopalan, and K. Smith, *Tools for Designing Thermal Management of Batteries in Electric Drive Vehicles (Presentation)* (National Renewable Energy Lab.(NREL), Golden, CO (United States of America)) (2013), https://www.osti.gov/biblio/1064502.
68. F. Ladrech, "Battery thermal management for HEV & EV–Technology overview." *Automotive summit* (2010).
69. Bdew (2017), Federal Association of the German Energy and Water Industries, Standard Load Profile H0., https://www.bdew.de/energie/standardlastprofile-strom/.
70. German Aerospace Center (DLR), Greenius - The Green Energy System Analysis Tool, http://freegreenius.dlr.de.
71. M. A. Awadallah, B. Venkatesh, E. Tolentino, and G. Thompson, *Journal of Energy Storage*, **13**, 425 (2017).